Diambra, A., Ibraim, E., & Camacho Tauta, J. (2019). Effect of orientation of principal stress axes on cyclic liquefaction potential of soils. In H. Sigursteinsson, S. Erlingsson , & B. Bessason (Eds.), *Proceedings of the XVII ECSMGE-2019* The Icelandic Geotechnical Society.

Proceedings of the XVII ECSMGE-2019
Geotechnical Engineering foundation of the future
ISBN 978-0-7277-6067-8

doi: 17ecsmge-2019-Y-XXXX

XVII European Conference
ECSMGE 2019
Reykjavík
on Soil Mechanics
and Geotechnical Engineering

Effect of orientation of principal stress axes on cyclic liquefaction potential of soils

Effet de l'orientation des principaux axes de contrainte sur le potentiel de liquéfaction cyclique des sols

A. Diambra,
University of Bristol, Bristol, United Kingdom

E. Ibraim
University of Bristol, Bristol, United Kingdom

J. Camacho-Tauta
Universidad Militar Nueva Granada, Bogota', Colombia

ABSTRACT: Soil liquefaction is a large loss of strength and stiffness induced by pore pressure build up often triggered by cyclic motions such as earthquakes. Its occurrence has historically created major collapses and life losses worldwide. Different laboratory techniques have been employed to estimate the cyclic stress ratio to produce soil liquefaction, imposing variation of either shear and normal stresses. However, rotation of principal stress axes invariably occurs during cyclic earthquake motion but this aspect, which has been noted to have a major effect, has not been yet appropriately investigated. Using the Hollow Cylinder Torsional Apparatus, this research has investigated how varying the orientation of principal stress axes (with respect to the material axes) can affect the liquefaction potential of soils. The results of experimental programme demonstrate that there is a critical orientation of principal stress axes, different from the commonly employed triaxial or simple shear conditions, for which a minimum cyclic stress ratio is obtained.

RÉSUMÉ: La liquéfaction du sol est une perte importante de résistance et de rigidité induite par une augmentation de la pression interstitielle, souvent déclenchée par des mouvements cycliques tels que les tremblements de terre. Son apparition a historiquement provoqué des effondrements majeurs et des pertes de vies dans le monde entier. Différentes techniques de laboratoire ont été utilisées pour estimer le rapport de contrainte cyclique afin de produire une liquéfaction du sol, imposant une variation des contraintes de cisaillement et normales. Cependant, la rotation des principaux axes de contrainte se produit invariablement pendant le mouvement sismique cyclique, mais cet aspect, qui a été noté comme ayant un effet majeur, n'a pas encore été étudié de manière appropriée. À l'aide de l'appareil de torsion à cylindre creux, cette recherche a permis de déterminer dans quelle mesure la modification de l'orientation des principaux axes de contrainte (par rapport aux axes des matériaux) peut affecter le potentiel de liquéfaction des sols. Les résultats du programme expérimental démontrent qu'il existe une orientation critique des principaux axes de contrainte, différente des conditions de cisaillement triaxial ou simple couramment utilisées, pour laquelle un rapport de contrainte cyclique minimal est obtenu.

Keywords: Liquefaction; Multiaxial stress; Sands; Cyclic loading; Hollow cylinder Torsional apparatus.

1 INTRODUCTION

Soil liquefaction is a large loss of strength and stiffness induced by pore pressure build-up often triggered by earthquakes. Its occurrence has historically created major collapses and life losses worldwide. Both laboratory and in-situ investigation techniques have been employed to determine the soil susceptibility to liquefaction and to estimate the triggering stress conditions. The laboratory-based techniques make use of different cyclic testing methods. The two most commonly employed methods are the cyclic triaxial test and the cyclic torsional shear test. However, actual earthquake actions on soil deposits are more complex than the stress conditions that these laboratory apparatuses can apply. The main difference stands on the so-called rotation of principal stress axes caused by the combination of cyclic vertical and horizontal stresses during the ground motion. Neither cyclic triaxial test nor cyclic torsional shear test are able to reproduce the re-orientation of principal stress axes during the cyclic motion.

Initial studies of the problem have been carried out by Ishihara et al. (1985) and Sivathayalan et al. (2014) showing that the direction and rotation of principal stress axes with respect to material axis (i.e. direction of soil deposition) have a marked influence on the number of cycles to attain the liquefied state. Ishihara et al. (1985) found that the cyclic stress ratio to cause liquefaction is significantly reduced if continuous rotation of principal stress axes is applied (i.e. a circular stress path in which the triaxial mode and the torsional mode are cyclically applied with a phase difference of 90˚). Sivathayalan et al. (2014) found that continuous rotation of principal stress is more detrimental than a sudden jump of principal stress direction. The authors observed the lowest cyclic resistance for tests where the continuous rotation of principal stress axes has a magnitude between ±45˚ and ±60˚.

This research will complement the scarcity of the available data on this important issue governing the liquefaction susceptibility of granular soils by providing new laboratory experimental data. The paper will show how the liquefaction susceptibility is affected by the orientation of the principal stress axes with respect to the material depositional bedding. Experimental tests have been performed using the Hollow Cylinder Torsional Apparatus (HCTA) at the University of Bristol. The experimental results will also show that the use of conventional cyclic triaxial test and torsional shear tests may not lead to a safe estimation of the liquefaction potential: there are particular orientations of principal stress axes for which a lower cyclic liquefaction resistance was observed.

2 MATERIAL

Red Hill 110 silica sand was used in this investigation. The sand is generally characterised by sub-rounded particle shape. The grain size distribution is provided in Figure. 1. Its physical properties are as follows: mean grain size D_{50}=0.17 mm, coefficient of uniformity Cu=2.25, coefficient of gradation Cg=1.17, specific gravity Gs=2.65 and minimum and maximum void ratios, respectively e_{min}= 0.608 and e_{max}= 1.035.

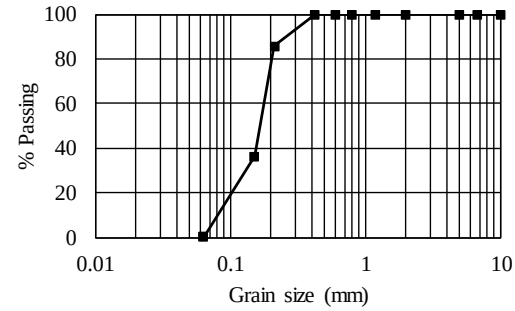

Figure 1. Particle size distribution fort Red Hill 110 silica sand.

3 EQUIPMENT

The HCTA provides a great freedom to explore general stress and strain soil behaviour and it is particularly suited for the investigation of the mechanical response under cyclic loading conditions. The apparatus has the capability to control axial load (*W*), torque load (*T*) and internal and external pressure (*Pi* and *Po*) independently (Figure 2a). The application of these enables the control of all the stress components: axial (σ_z), radial (σ_r), circumferential (σ_θ) and shear stress ($\tau_{\theta z} = \tau_{z\theta}$) on an element of the hollow cylindrical specimen (Figure 2b). Under undrained conditions, changes in stresses builds up excess of pore pressure (μ). The stress path can be characterised by four independent parameters, such as the mean principal effective stress *p' (1)*, generalised deviatoric component of stress q_g *(2)*, intermediate principal stress parameter *b (3)* and the angle α_σ *(4)* between the major principal stress σ_1 and the vertical direction (Figure 2c), defined as:

$$p' = \frac{\sigma_z+\sigma_\theta+\sigma_r}{3} - \mu = \frac{\sigma_1+\sigma_2+\sigma_3}{3} - \mu \quad (1)$$

$$q_g = \sqrt{\frac{(\sigma_z-\sigma_r)^2+(\sigma_r-\sigma_\theta)^2+(\sigma_\theta-\sigma_z)^2}{2} + 3{\tau_{\theta z}}^2} \quad (2)$$

$$b = \frac{\sigma_2-\sigma_3}{\sigma_1-\sigma_3} \quad (3)$$

$$\alpha_\sigma = \frac{1}{2}\, tan^{-1}\left(\frac{2\tau_{\theta z}}{\sigma_z-\sigma_\theta}\right) \quad (4)$$

Variations in the stress state produces deformations of the specimen, which can be expressed in terms of axial (ε_z), radial (ε_r), circumferential (ε_θ), and shear ($\gamma_{\theta z}$) strains. The deviatoric strain (ε_q), which is related to deformation at constant volume can be computed as:

$$\varepsilon_q = \frac{1}{3}\sqrt{4(\varepsilon_z-\varepsilon_r)^2 + 3{\gamma_{\theta z}}^2} \quad (5)$$

Soil samples tested in the HCTA have a typical hollow cylindrical shape. The specimens have an outer radius (r_o) of 50mm, inner radius (r_i) of 30mm and 200mm height (*H*) as shown in Figure. 2a. The geometry helps minimizing the degree of stress and strain non-uniformities, inevitable in a hollow cylinder specimen as a result of the sample curvature and the restraint at its ends (Sayão and Vaid, 1991; Hight et al., 1983). Further details of the testing apparatus can be found in Mandolini et al. (2018).

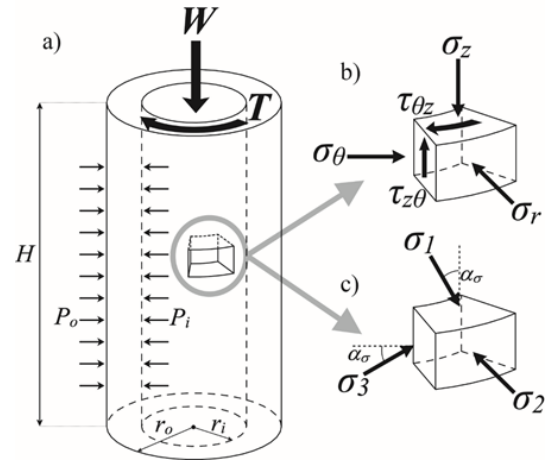

Figure 2. Stress state in hollow cylinder torsional sample (a). Details of the element in the wall: the (b) stress components and (c) main principal stresses.

4 SAMPLE PREPARATION

Specimens of sand were prepared by dry pluviation (similarly to Escribano et al. 2018). Oven-dried Red hill 110 sand was gently poured into the mould through a funnel. The pouring tip was continuously moved up with the surface of the deposit maintaining a constant zero fall height. Small vibration was finally applied to the sample if the denser target density has to be achieved. The samples were tested in fully saturated conditions which were ensured by CO_2 flushing method together with employment of water back pressure up to 300 kPa. Once saturated, the specimen was subjected to an isotropic consolidation performed by manually increasing the cell confining pressure. A picture

of a prepared hollow cylindrical sample is provided in Figure 3.

Figure 3. Image of prepared hollow cylindrical sample.

5 TESTING PROGRAM

The experimental testing programme consisted in the performance of eight cyclic undrained tests imposing different values of the orientation of the major principal stress direction, α_σ, at two different value of cyclic stress ratio (CSR). The cyclic stress ratio is defined here as:

$$CSR = \frac{q_{cyc}}{p'_0} \quad (6)$$

where q_{cyc} is the length of the cycles in the $\tau_{\theta z}$, q plane where q is the difference between the axial and radial stress in the sample:

$$q = \sigma_z - \sigma_r \quad (7)$$

The cyclic tests have a symmetric shape with respect to the origin of the $\tau_{\theta z}$-q stress plane, as it will be shown in the stress paths in the following section 6.

The tests have been carried out on samples with a nominal relative density of about 50% and under an effective cell confining pressure of 50 kPa, to which the samples have been consolidated prior to cycling. Specific details of the performed tests are reported in Table 1 where the number of cycles to reach liquefaction is also shown. Liquefaction is reached when the excess pore pressure rises so much that the effective average stress becomes zero.

The number of cycles to liquefaction has been determined taking into account the compliance due to the membrane stiffness (Tokimatsu and Nakamura, 1987).

The cyclic tests have been carried out at a frequency of 0.1 Hz. Axial and torque loads follow a sinusoidal waveform and when simultaneously applied, they are in phase (i.e. maximum amplitudes are reached at the same time).

Table 1.List of tests performed in the experimental programme

Name	CSR	$2\alpha_\sigma$	D_r (%)	No. cycles
T0.12_00	0.12	0°	49	83
T0.12_30	0.12	30°	51	26
T0.12_60	0.12	60°	50	43
T0.12_90	0.12	90°	59	132
T0.16_00	0.16	0°	49	12
T0.16_30	0.16	30°	48	7
T0.16_60	0.16	60°	49	14
T0.16_90	0.16	90°	60	27

6 TEST RESULTS

The typical stress paths applied to the samples are shown in Figure 4 for the series of tests at both *CSR*=0.12 and *CSR*=0.16. Slight deviation from a perfectly linear stress paths are obviously due to minor inaccuracies in the simultaneous control of torque and axial force. Nevertheless, the samples followed quite closely the desired stress paths.

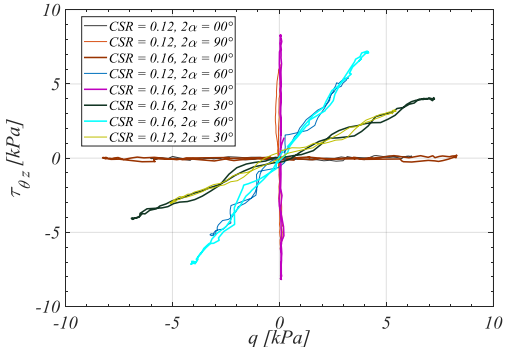

Figure 4. Stress paths followed by samples tested at CSR=0.12 and CSR=0.16 in the $\tau_{\theta z}$ -q plane.

Typical deviatoric stress-strain behaviour recorded during the undrained cyclic loading is reported in Figure 5. The behaviour is characterised by an initial stiff response with limited accumulation of plastic deviatoric strain (ε_q) up until the triggering of liquefaction conditions. This is in agreement with both experimental and theoretical findings (e.g. Seed and Lee 1966, Corti et al. 2016, Liu et al. 2018)

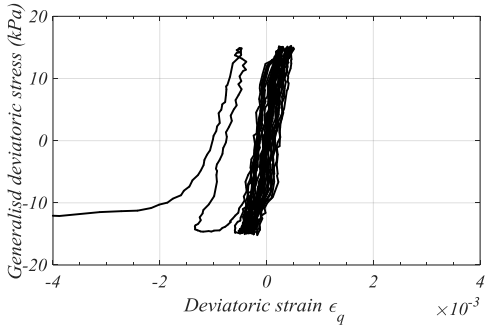

Figure 5. Generalised deviatoric stress-strain behaviour for samples T0.16_60.

As expected, progressive pore water pressure build up occurred during the undrained cyclic stage for all the tests. The typical effective stress paths followed in the $\tau_{\theta z}$ *-p'* for a sample tested at $2\alpha_\sigma$ =90˚ is shown in Figure 6. A larger accumulation of pore water pressures takes place in the first and second cycle, followed by very close cycles with limited decrease of mean effective stress up to about two three cycles before liquefaction, when larger pore water pressure build-up can be recorded.

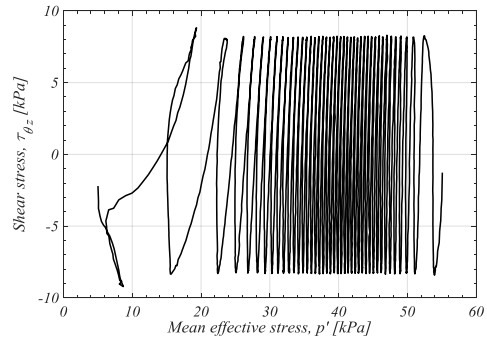

Figure 6. Stress path in the τ-p' stress plane followed by sample T0.16_60

The progressive accumulation of excess pore water pressure with the increasing number of cycles can be better visualised in Figure 7. Such figure can be conveniently used to determine the number of cycles to trigger liquefaction, at the net of corrections due to the membrane compliance.

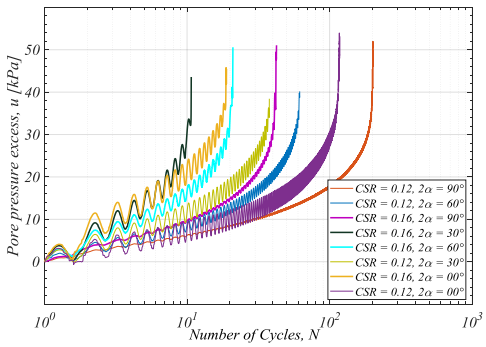

Figure 7. Evolution of excess pore water pressure for all the samples tested in the experimental programme.

The number of cycles to trigger liquefaction are plotted in Figure 8 versus the inclination $2\alpha_\sigma$ of the principal stress axes. Despite some limited differences in the relative density of the sample, it is clear that orientations of principal stress axis different from pure compression ($2\alpha_\sigma$=0˚) and pure torsion ($2\alpha_\sigma$=90˚) lead to an anticipated occurrence of liquefaction – i.e. liquefaction is attained at a lower number of cycles. The lowest resistance is observed at around 15˚ inclination of the major principal stress axis with vertical axis, which is the axis perpendicular to the soil depositional bedding. The maximum resistance appears to be related to pure torsional loading mode, although it should be noted that these samples were slightly denser than the others.

If the number of cycles is normalised with respect to the number of cycles for pure torsion, the trends in Figure 9 can be obtained. It appears that the cycles for triggering liquefaction at $2\alpha_\sigma$=30˚ are about 1/5 of those for the pure torsional mode. While this measure can be affected by the differences in density, the ratio with the pure compressive mode would still be in the order of 2 to 3.

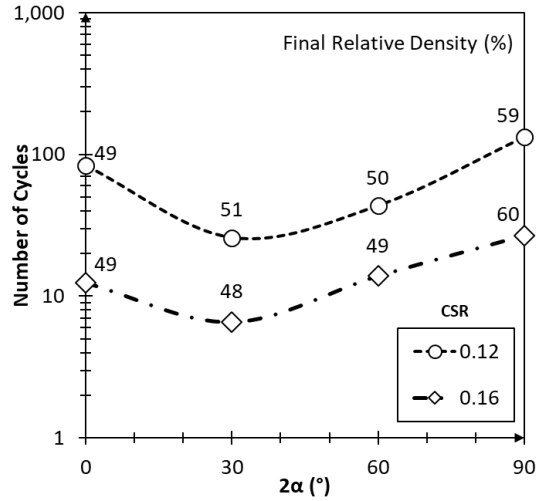

Figure 8. Variation of number of cycles versus the orientation of principal stress axes $2\alpha_\sigma$.

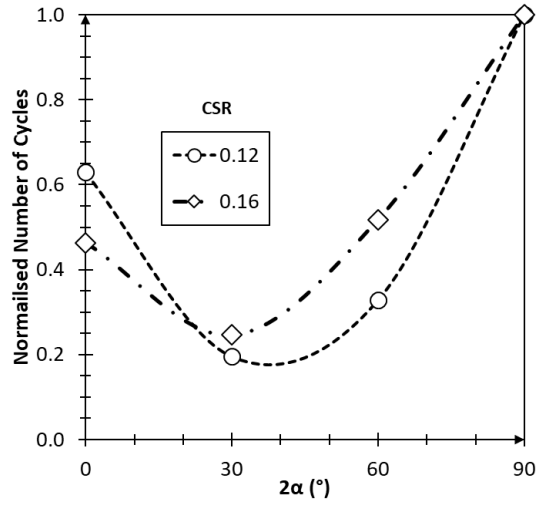

Figure 9. Variation of normalised number of cycles (defined as the ratio between the No. cycles divide by the No cycles for the pure torsional mode) versus the orientation of principal stress axes $2\alpha_\sigma$.

The related CSR curves with the number of cycles for the different values of orientation of principal stress axes $2\alpha_\sigma$ are shown in Figure 10. Variations of the principal stress orientation cause a leftward shift to the curves, with the lowest resistance curve observed for the

orientation of 30˚. Indeed, further confirmation testing sample for a larger range of CSRs is required to complete these curves and to identify whether the required critical stress ratio can be extrapolated beyond the testing conditions of this experimental programme.

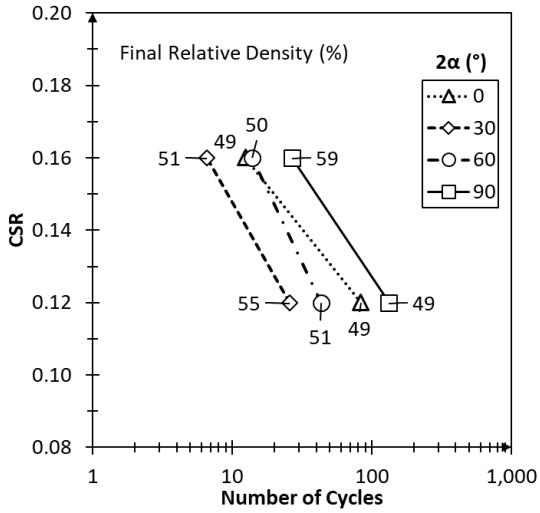

Figure 10. CSR curves versus number of cycles to trigger liquefaction for different orientation of principal stress axes $2\alpha_\sigma$.

7 CONCLUSIONS

This paper has presented some experimental results to investigate the cyclic liquefaction susceptibility of granular soil in the multiaxial stress space. Particular emphasis has been directed towards the investigation of the effect of the direction of principal stress axis with respect to material depositional bedding. It was found that common procedures to demine the liquefaction resistance using pure compressional or torsional cycling do not lead to conservative estimations of the number of cycles to liquefaction. In this investigation, it was found that the lower resistance to liquefaction was observed around 15˚ inclination of the principal stress axes from the axes of material depositional bedding.

Further tests should be carried out to extend the loading conditions of this research and to investigate whether a unique relationship between normalised number of cycles and orientation for principal stress axes can be identified.

8 ACKNOWLEDGEMENTS

The authors are very grateful to the financial support of the British Council Newton Fund - Grant Reference: RLTG6 – 261594280 - which allowed the research visit and performance of the experimental programme of Dr Camacho-Tauta at University of Bristol. Academic leave for this visit was possible thanks to the project IMP-ING-2131 funded by the Research Direction of Universidad Militar Nueva Granada

9 REFERENCES

Corti, R., Diambra, A., Wood, D.M., Escribano, D.E., Nash, D.F., 2016. Memory surface hardening model for granular soils under repeated loading conditions. Journal of Engineering Mechanics, 142(12), DOI: 10.1061/(ASCE)EM.1943-7889.0001174.

Escribano, D., Nash, D., & Diambra, A. (2018). Local and global volumetric strain comparison in sand specimens subjected to drained cyclic and monotonic triaxial compression loading. *Geotechnical Testing Journal 42(4).* DOI: 10.1520/GTJ20170054

Hight, D.W., Gens, A., Symes, M.J. 1983. The development of a new hollow cylinder apparatus for investigating the effects of principal rotation in soils. Géotechnique **33**(4), 355-383.

Mandolini, A., Diambra, A., Ibraim, E. 2018. Strength anisotropy of fibre-reinforced sands under multiaxial loading. Géotechnique, 1-14. https://doi.org/10.1680/jgeot.17.P.102

Ishihara, K., Towhata, I., Yamazaki. A. 1985. Sand liquefaction under rotation of principal

stress axes. Proc. ICSMFE, Vol. 2. 1985, 1015-1018.

Liu, H. Y., J. A. Abell, A. Diambra, & F. Pisano (2018). Modelling the cyclic ratcheting of sands through memory-enhanced bounding surface plasticity. *Géotechnique* DOI: 10.1680/jgeot.17.P.307.

Sayão, A., Vaid, Y.P., 1991. A critical assessment of stress non-uniformities in Hollow Cylinder Test Specimens, Soils and Foundations, Vol. **31**(1), 61-72.

Seed, B. and Lee, K.L., 1966. Liquefaction of saturated sands during cyclic loading. Journal of Soil Mechanics & Foundations Div, 92 (ASCE 4972 Proceeding).

Sivathayalan, S., Logeswaran, P., Manmatharajan, V. 2014. Cyclic resistance of a loose sand subjected to rotation of principal stresses. Journal of Geotechnical and Geoenvironmental Engineering, **141**, (3), 04014113.

Tokimatsu, K. and Nakamura, K. 1987 A simplified correction for membrane complience in liquefaction tests. Soils and Foundations, **27**, (4), 111-122.